IEEE Access
Multidisciplinary ⋮ Rapid Review ⋮ Open Access Journal

Received 13 November 2023, accepted 28 November 2023, date of publication 1 December 2023,
date of current version 12 December 2023.

Digital Object Identifier 10.1109/ACCESS.2023.3338724

RESEARCH ARTICLE

Optical Characteristic Measurement of Micro/Nanodroplet on Embedded Grating Nanostructure for Digital Microfluidic's Electrode

AMILLA PUSPADUHITA[1,2], AKHMADI SURAWIJAYA[3], (Member, IEEE), AND ISA ANSHORI[2,4]

[1]Department of Nanotechnology, Graduate School, Institut Teknologi Bandung (ITB), Bandung 40132, Indonesia
[2]Research Center for Nanoscience and Nanotechnology, Institut Teknologi Bandung (ITB), Bandung 40132, Indonesia
[3]Department of Electrical Engineering, School of Electrical Engineering and Informatics, Institut Teknologi Bandung (ITB), Bandung 40132, Indonesia
[4]Lab-on-Chip Group, Department of Biomedical Engineering, School of Electrical Engineering and Informatics, Institut Teknologi Bandung (ITB), Bandung 40132, Indonesia

Corresponding author: Akhmadi Surawijaya (asurawijaya@itb.ac.id)

This work was supported by the Institut Teknologi Bandung (ITB) Young Faculty Member Research under Grant LPPM.PN-6-29-2022.

ABSTRACT This report describes the potential design of an optical sensor system, in which the localized surface plasmon resonance (LSPR) type was used, coupled with digital microfluidic (DMF) technology. To achieve this potential design, a dielectric material was layered on top of a metal grating nanostructure so that the nanostructure was embedded in the dielectric matrix. Then, a hydrophobic layer was stacked on top of the dielectric layer for micro/nanodroplet movement. Sensitivity and figure of merit (FoM) parameters were analyzed to evaluate this potential design. In this research, various kinds of metal were investigated, and it was found that a gold grating nanostructure embedded inside the SiO_2 dielectric matrix with Teflon AF2400 as hydrophobic layer gave the optimum sensitivity. However, the iron grating nanostructure embedded inside the SiO_2 dielectric matrix with Teflon AF2400 as hydrophobic layer gave the optimum FoM of 1.481. Furthermore, noble metal grating nanostructures embedded inside a dielectric layer produce higher photoelectric conversion and current density values than other types of metals that are usually used, such as aluminum, cobalt, iron, copper, etc.

INDEX TERMS Digital microfluidic, embedded grating nanostructure, figure of merit, localized surface plasmon resonance, sensitivity.

I. INTRODUCTION

Depending on what application of the device is, the choosing of materials and the size would affect the characteristics of a certain device, so this process should be done very carefully in order to minimize the potential side effects in the device. Some of these material properties and characteristics were observed using certain methods, such as electron and optical microscopic, diffraction, spectroscopy, thermal, electrical, magnetic, and mechanical experiments [1]. These methods require a massive size of equipment and are not suitable for usual use, especially for the field usage. To overcome this limitation, researchers develop sensor technology to do material characterization processes. This technology has some advantages, especially for its fast response time and on-site usage. Furthermore, the development of nanotechnology also influences the development of sensor technology, which gives improvements on its sensing performances.

Based on characteristics and main application, a sensor is classified into some types, they are based on its measurand (A), technological aspects (B), detection means used (C), sensor conversion phenomena (D), materials (E), and fields of application (F) [2]. In this work, the sensor system was classified as such: A7.1 Wave amplitude, phase (Optical); B1 Sensitivity and B12 Figure of Merit (FoM); C3 Electric, magnetic, or electromagnetic wave; D3.2 Photoelectric; E1 Inorganic; and F16 Materials characterization.

Optical sensor is a type of a sensor that convert light to electrical signals because of the photoelectric effect. The presence of an analyte will change the transmittance, reflectance,

The associate editor coordinating the review of this manuscript and approving it for publication was Santosh Kumar.

absorbance, luminescence, or refractive index parameters which give the different output signal as well [3]. Optical sensor was fabricated based on some phenomenon, such as surface plasmon resonance (SPR), fluorescence, radiolabeling, refractive index variations, refractometry, ellipsometry, and evanescent wave. This type of sensor has some advantages, such as real-time and in-situ detection, potential in miniaturization and simultaneous detection [4]. This work utilizes SPR phenomenon, specifically localized SPR (LSPR) as a sensor system. SPR is an optical phenomenon where an electron on a metal surface was excited by a photon with a certain incident's angle, then parallelly spread on the metal surface [5]. There are some types of SPR configurations, such as grating, prism coupler, waveguide, and LSPR [6]. The main difference between LSPR and the other types of SPR sensor is the exploitation of nanoparticles instead of thin film. Nanoparticles also produce SPR, but the resonance wavelength would be localized inside a nanoparticle or a nanostructure [7]. There are two types of LSPR setup, they are transmission based and reflectance based.

Digital microfluidic is a platform that could potentially realize a lab-on-a-chip system. The groundwork of this technology is the manipulation of a certain amount of a droplet on top of a surface through a few mechanisms, such as electrowetting, dielectrophoresis, thermocapillary transport, and surface acoustic wave (SAW) transport. The digitalization part in this technology is about the utilization of array of electrode combinations to control some of the droplet parameters, such as position and hydrophobicity [8]. There are a few main components that construct a digital microfluidic device, there are substrate, electrode and its configuration, dielectric material and its thickness, hydrophobic material and its thickness, and also the voltage applied to the device [9].

To integrate an optical sensor system and DMF technology, there are some things that should be considered carefully, such as structural design parameters, materials choosing, and fabrication technique. Straight canal structure is one of the easiest designs to fabricate, it's also simple and suitable for DMF systems [10]. There are some suitable materials for DMF fabrication, which also act as a substrate for an optical sensor system. They are metals, ceramics, glasses, composites, elastomers, thermoplastics, and papers. Glasses were used as a substrate because of low prices, but it was hard to produce on a smaller scale. To substitute it, elastomers, and thermoplastics such as polydimethylsiloxane (PDMS) was used, not only because of its light weight, but also transparent and resistant to deformation, which was very ideal for optical sensor system [11]. Lastly, there were lots of fabrication techniques to produce a certain structure, for example, using templating and 3D printing. Templating usually was conducted using silicon wafer, then elastomers such as PDMS was poured over the template. On a smaller scale, fabrications were conducted using electron beam lithography (EBL), focused ion beam lithography (FIB), nanoimprint lithography (NIL) techniques, etc. Especially for biomarkers detection, structures, materials, and fabrication techniques were focused on the device compatibility with the biomarker and its environment [12], [13]. There were already works that integrated optical sensor system with digital microfluidic technology, one of them is colorimetry coupled with ITO arrays of electrode based on active matrix electrowetting-on-dielectric (AM-EWOD) which could detect glucose in a human blood serum. It could reach the limit of detection (LoD) of 33 μM [14]. Colorimetry coupled with arrays of gold electrode also could detect nitrite with the LoD of 13 μg/L [15]. Another one is 58 actuator electrode and 3 reservoir electrode EWOD-based DMF technology coupled with colorimetry using AuNP could detect Hg^{2+} with the LoD of 0.01 μM [16]. Other than calorimetry, there were other types of optical sensor system that could be integrated with DMF technology that has also been researched, one of them is optical resonator. Nanophotonic microring resonator coupled with aluminum actuator electrode using EWOD-based could conduct multidetection system of glucose, NaCl, and ethanol with the sensitivity of 77$\pm$0.6 nm/RIU [17]. Optical microdisk resonator integrated with metal (Pt/Ti) on SiO_2/Si substrate could detect glucose with the sensitivity of 69 nm/RIU and FoM of 197 [18]. SU-8 polymer optical resonator coupled with Chromium EWOD-based DMF could detect D-glucose with the sensitivity of 20 nm/RIU [19]. Based on the development of optical sensor systems integrated with DMF technologies, however, there was no research yet about integrating LSPR sensors with DMF technologies and its optimization. Furthermore, the optical sensor system and DMF part usually was separated into a few chambers in most studies. In this study, we proposed an embedded grating nanostructure which could be integrated between two digital microfluidic's electrodes. This research was conducted by simulation using ANSYS Lumerical FDTD.

II. DESIGN AND PARAMETERS

A. PROPOSED STRUCTURE OF OPTICAL SENSOR SYSTEM USING EMBEDDDED GRATING NANOSTRUCTURE

In this research, the optical sensor system integrated with DMF technology was proposed in Figure 1.

The optical sensor system design proposed was supposed to be among the arrays of DMF electrodes. The droplets that came from the inlet would move on the device, and when it arrived on the optical sensor system, it would stop, and the detection process of the droplet would begin. In the optical sensor part, there were some main components that should be addressed further, such as substrate, embedded grating nanostructure, dielectric layer, hydrophobic layer, and analyte. The structure of the optical sensor system design with and without embedded grating nanostructure will be presented in Figure 2 and Figure 3.

B. MAIN COMPONENTS OF BASIC DESIGN AND OPTIMIZATION

After modelling the structure for simulation, each material parameter should be added according to the structure. Based

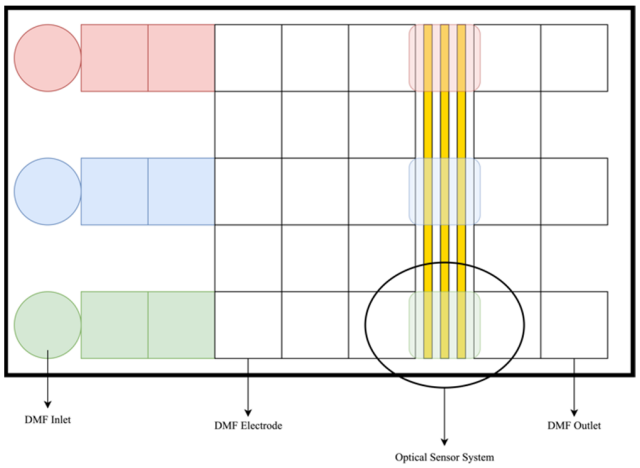

FIGURE 1. Proposed design of optical sensor system integrated with DMF technology.

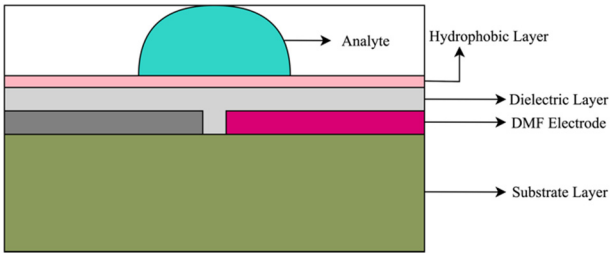

FIGURE 2. DMF technology design without optical sensor system.

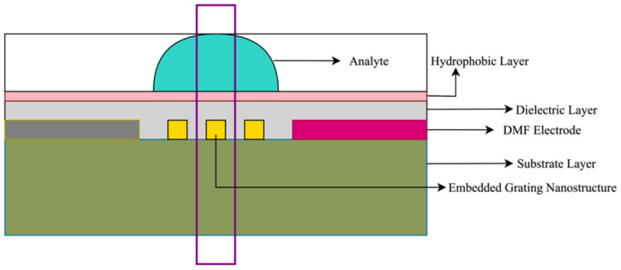

FIGURE 3. Proposed design of optical sensor system integrated with DMF technology. The optical sensor part consists of substrate layer, embedded grating nanostructure, dielectric layer, hydrophobic layer, and analyte. This part was obtained from FIGURE 1 inside the purple circle.

on optical characteristic, each materials have refractive index of complex number n, where the real part of n was described as quantization of light velocity's reduction when light passes through more polarized materials rather than vacuum. The imaginary value of n, represented as k, was described as quantization of light attenuation in the materials because of absorption. The complete refractive index equation was described as such:

$$n = n + ik \tag{1}$$

Usually, increased k value will lead to more opaque materials. However, this trend would not always true to every wavelength because of dispersion characteristics would vary, meaning that the transparency of materials was affected by the comparison between the effect of real and imaginary value for every wavelength in every material [20], [21]. In this section, we will further discuss the optical characteristics of the materials used to build the optical sensor system's design.

The first one is substrate layer. Substrate layer has a main purpose as a medium to put nanostructure. Usually, glass and silicon were used because of its sturdy, stable, and consistent characteristics. However, upon further inspection, this material has high energy loss when reduced to nanometer size. That's why there were lots of research to find the perfect substitute for this material. Some of the materials proposed in the research were indium tin oxide (ITO), polyethylene terephthalate (PET), polystyrene (PS), indium phosphate (InP), polydimethylsiloxane (PDMS), etc. This research uses PDMS as a substrate not only because it has suitable optical characteristics, but also it has a lot of potential in the development of a flexible sensor system [22]. The suitable optical characteristic of PDMS is marked by modest but discernible anisotropy, with values of ∼6.2/25% for the dielectric constant and loss tangent, respectively. This optical property gives advantage to the bending effect so that when bending occurs, the anisotropy effect of dielectric constant can be balanced on the substrate's surface [23]. The transparency and hydrophobicity of PDMS also led some researchers to utilize it as both dielectric layer and hydrophobic layer [24], [25]. The parameters of this material were obtained from research where this material was fabricated using the ratio of main:curing agent of 10:1 and it was measured at normal temperature and pressure. The thickness of the substrate was set to 100 nm [26]. This value was chosen because as of now, the thinnest PDMS substrate layer that could be fabricated for flexible sensor purpose has a thickness value of around 100 nm [27].

The next component is nanostructure. There are lots of shapes and size that could be used in this research. However, this research will focus on developing optical sensor system using grating nanostructure. The type of materials used in this research is metallic, especially the ones that are often used for sensor development. Those materials are silver (Ag), aluminum (Al), gold (Au), cobalt (Co), copper (Cu), iron (Fe), nickel (Ni), palladium (Pd), and zinc (Zn) [28], [29]. The optimization for this structure was done for the width of the gold grating nanostructure, then variation of the materials would be investigated to obtain the most optimum result. The thickness of the grating nanostructure was set to 30 nm. This value was used to match the thinnest DMF electrode that had ever been fabricated at room temperature before using Indium Tin Oxide (ITO) [30].

The dielectric layer actually has a main purpose to build charge and electric field gradients on the DMF device. Furthermore, this layer also prevents electrolysis and restricts the electric current flow to flow through only in the electrode [31], [32]. The materials used for this layer are usually from silicon nitride, silicon oil, decane, hexadecane, etc [33]. On the optical sensor system part, the dielectric layer added

on the nanostructure could give some advantages, especially for protecting the nanostructure by increasing the thermal and oxidative stability [34], [35]. The next development for this structure could be for fabricating a detection system that could be used repeatedly instead of only once. Furthermore, some dielectric materials could also add the reactivity of metal nanostructure embedded in the dielectric layer [31]. In this research, there were some dielectric materials that would be investigated, such as CdS, CdSe, PbS, SiO_2, ZnO, and WO_3 [36], [37], [38], [39], [40], [41]. In this research, the thickness of dielectric layer was set to 50 nm. This value also referred to the thinnest of these dielectric materials proposed that could be fabricated with an embedded structure as of now [42], [43], [44].

Hydrophobic layer is the uppermost layer of the DMF that has a direct contact with the analyte. This hydrophobic layer has a main function to lower the surface energy of the analyte and the device's surface [45]. Then, the voltage that was applied to activate the electrode will change the wettability rate of the analyte and the device [46]. In this way, the analyte can move according to which electrode was activated. There were lots of materials that could be used as hydrophobic layer for DMF device, such as Teflon AF, Parylene C, Cytop, PDMS, polytetrafluoroethylene (PTFE), and many more [47], [48], [49]. In this research, the materials that would be investigated were Teflon AF with three grades, 1300, 1601, and 2400 [50]. Teflon AF was chosen for this research because it's easy to obtain, and there were some variations of grades that we could investigate further so that the design proposed could produce optimum performance. The thickness was also set to 12 nm in this research. It referred to the optimum thickness of hydrophobic layer for the EWOD system obtained from research of Teflon AF and Cytop [47]. Both materials have the critical thickness, meaning the minimum value of thickness in which it could produce hydrophobic characteristics. The critical thickness of Cytop and Teflon AF is 3 nm and 7 nm, respectfully. When these materials have a thickness of more than 12 nm, the hydrophobicity would decrease.

In this research, there were two analytes used to investigate the performance of the device. They were blood and water [51], [52].

C. SIMULATION AND PERFORMANCE PARAMETERS

There were some main parameters that should be considered in this research, such as reflectance, transmittance, excitation source, field monitor, FDTD, meshing, optical power absorption. The general setup of the simulation on the ANSYS Lumerical FDTD's window was attached in Figure 4.

The simulation was done in 3D simulation type, the boundary condition of the X and Y axis is periodic, and for the Z axis is a perfectly matched layer (PML). PML was used to reduce back reflection [53]. The wavelength used in this simulation was in the range of 300 nm to 2500 nm. This range of value was used to investigate the behaviour of the

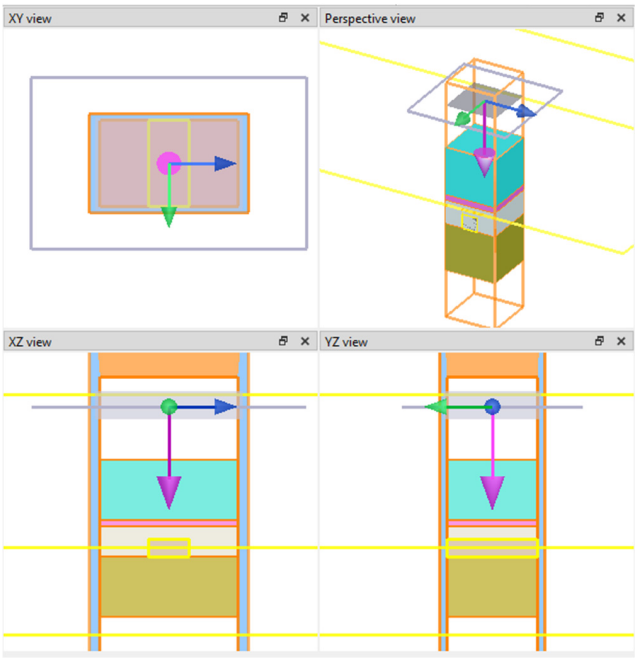

FIGURE 4. General simulation setup in this research using ANSYS Lumerical FDTD.

structure when exposed to different wavelengths (near ultraviolet (UV), visible light, near-infrared (IR), and mid-IR) so that the data obtained from this research could act as a reference to determine which light source that could produce the optimum detection results for the experiment setup. The mesh step was calculated using the following equation:

$$N_\lambda = \frac{\lambda}{\Delta x \cdot n} \tag{2}$$

where the Δx represent the mesh step across a dimension of a lattice, λ represent the smallest wavelength from the excitation source used in the simulation, and n represent the highest value of the refractive index of the structure. The ideal mesh step has N_λ value of 10 to ensure the tradeoff between the accuracy and resource needed for 3D type of simulation [54]. However, in this research, N_λ value for embedded grating nanostructure would be set to more than 10 to make certain of the accuracy of the simulation.

Reflectance and transmittance profile was obtained by adding frequency domain power monitors on top of the excitation source and below the proposed design, respectively. Absorbance was obtained by using the following equation:

$$A = 1 - R - T \tag{3}$$

where R represent the reflectance, T represent transmittance, and the value 1 represent the 100% of light that was produced by the light source before passing through the optical sensor system.

Power that passes through an active region is described as absorption per unit volume. For ANSYS Lumerical FDTD, absorption per unit volume can be measured using advanced power absorbed objects from the object library. After the optical power value was obtained, optical generation rate, G,

represented as number of excited electrons per volume unit per time could be obtained from the following equation:

$$G(\vec{r},\xi) = \frac{P_{abs}(\vec{r},\omega)}{\hbar\cdot\omega} = \frac{P_{source}(\omega)}{\hbar\cdot\omega}\frac{P_{abs}^{FDTD}(\omega)}{P_{source}^{FDTD}(\omega)} \quad (4)$$

In which ω represent the angular frequency, $\hbar$ represent reduced Planck constant, $P_{abs}(\vec{r},\omega)$ represent the optical power absorbed. However, to calculate the generation rate of a real experimental setup, the normalized absorbed power,

$$\frac{P_{abs}^{FDTD}(\omega)}{P_{source}^{FDTD}(\omega)}$$

which is calculated from the FDTD simulation, should be multiplied by the experimental source power, P_{source} in *Watts*. In this research, the value of P_{source} was set to default of 1 *Watt* [54], [55].

After G value was obtained, photoelectric conversion (PC) could be calculated by integrating G value over the embedded grating nanostructure's volume. Then, the number of electrons can be converted to current by multiplying it by $q = 1,60217663 \times 10^{-19} C$.

$$PC = \int_V (G(\vec{r},\xi)\cdot q)dV \quad (5)$$

The assumption used by this conversion is that one photon can produce only one electron. To obtain current density, we will calculate the difference of photoelectric conversion value when blood and water is used as analytes, then dividing it by cross-sectional area of embedded grating nanostructure. Photoelectric conversion can be utilized to see where the wavelength can potentially produce the optimum current density that pass through the grating nanostructure's grid. This optimum current density corresponds to the optimum performance that could be achieved in a sensor system design [56].

There are lots of parameters that can be used to describe the performance of a sensor. However, only sensitivity and figure of merit (FoM) were used in this research. Refractive index sensitivity was measured by detecting the LSPR resonance peak shift when there is a change in the analyte's refractive index value. Refractive index sensitivity was calculated by the following equation:

$$S = \frac{\Delta\lambda}{\Delta n} \quad (6)$$

where λ represent the resonance wave peak wavelength and n represent the refractive index value of an analyte [57]. In this research, resonance peak wavelength was obtained from the LSPR absorbance peak wavelength profile.

LSPR detection is one of the detection techniques based on the wavelength peak shift. The precision level is determined from the sensitivity value and the width of the resonance wave peak line. Larger nanostructures tend to have a high sensitivity value, however, the peak produced is usually from multipolar excitation and damping radioactive. To confirm the detection capabilities of a nanostructure, FoM is obtained by dividing the sensitivity, S, by the resonance line width (FWHM):

$$FoM = \frac{S}{FWHM} \quad (7)$$

III. SIMULATION RESULTS AND DISCUSSION

A. OPTIMIZATION OF THE GOLD GRATING NANOSTRUCTURE'S WIDTH

In this first optimization step, gold grating nanostructure's optimum width was investigated without the dielectric and hydrophobic layer. The simulation setup was attached in Figure 5.

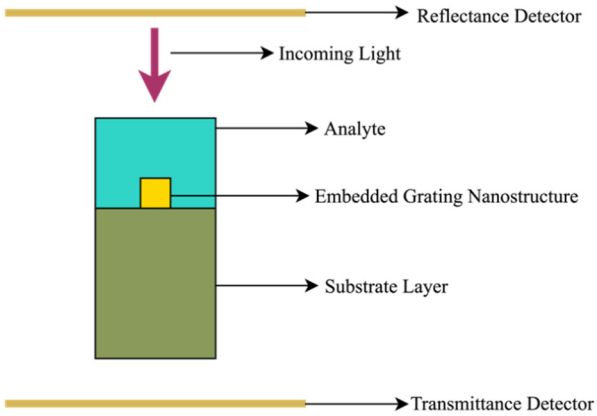

FIGURE 5. Simulation setup of the optimization of gold grating nanostructure's width.

Based on the structure above, the result of the detection performance by variating the grating nanostructure's width will be attached in Table 1.

TABLE 1. Gold grating nanostructure's width optimization.

Gold Nanograting Width (nm)	Performance	
	Sensitivity (nm/RIU)	*FoM*
10	1274.53	1.4
20	1127.31	1.52
30	1131.51	1.53
40	225.04	0.53
50	172.4	0.38
60	172.4	0.38
70	243.24	0.53
80	243.24	0.53
90	79.07	0.29

Based on the table above we could see that the optimum width is 30 nm. Furthermore, the FoM value obtained from the simulation was found within the range of the most single nanoarray-based LSPR sensor, which is 0.35 to 17. However, based on the complexity and the size of a nanostructure, single gold nanoarray usually has a very low FoM value below [58], [59], [60].

B. OPTIMIZATION OF DIELECTRIC LAYER'S MATERIAL

After optimizing the gold grating nanostructure's width, the effect of adding the dielectric layer was investigated. The dielectric layer covered over the gold grating nanostructure so that it was embedded inside the dielectric layer. The simulation setup was attached in Figure 6.

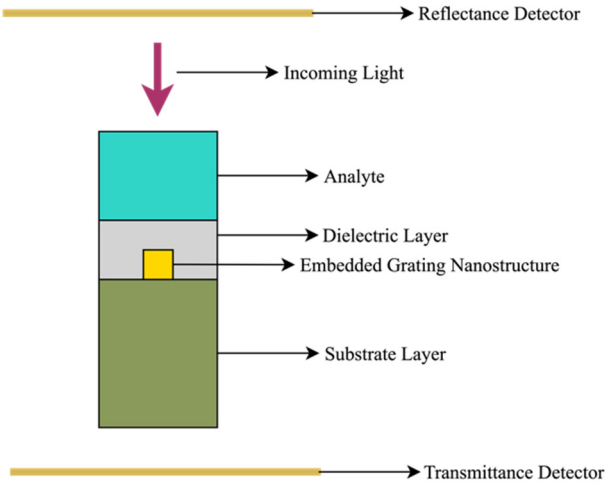

FIGURE 6. Simulation setup of the optimization of dielectric layer's material.

Based on the simulation setup above, the optimization of dielectric layer's material was attached in Table 2.

TABLE 2. Dielectric layer's material optimization.

Dielectric Material	Performance	
	Sensitivity (nm/RIU)	*FoM*
CdS	1245.47	1.31
CdSe	967.42	1.30
PbS	474.41	1.21
SiO_2	1979.22	2.22
ZnO	1739.04	2.13
WO_3	1660.73	1.87

From the result above, we could see that gold grating nanostructure embedded in SiO_2 dielectric material has the optimum performance in both sensitivity and FoM. Based on the optimization of gold grating nanostructure's width result, it could be concluded that adding SiO_2, ZnO, and WO_3 as dielectric layer can produce better performance rather than without adding the dielectric layer. In CdS, CdSe, and PbS, the k value of the refractive index of these materials are quite high, which means that these materials tend to be quite opaque. While in SiO_2, ZnO, and WO_3, the k values are very low, and the lowest k value was present in SiO_2 throughout the simulation wavelength range. Furthermore, SiO_2, ZnO, and WO_3 have the tendency to reduce bulk conductivity of embedded grating nanostructure so they can help the localization of the SPR phenomenon that happens inside the embedded gold grating nanostructure. In addition, SiO_2 has inert characteristics so that this material would never interfere with the internal reaction in embedded gold grating nanostructure.

TABLE 3. Embedded grating nanostructure's material's optimization.

Embedded Grating Nanostructure's Material	Performance	
	Sensitivity (nm/RIU)	*FoM*
Au	1979.22	2.22
Ag	1227.22	1.25
Al	1232.42	1.35
Co	1333.12	1.44
Cu	1292.88	1.41
Fe	1193.67	1.37
Ni	1209.44	1.36
Pd	1273.87	1.39
Pt	1282.92	1.41
Zn	1324.01	1.46

C. OPTIMIZATION OF THE EMBEDDED GRATING NANOSTRUCTURE'S MATERIAL

In this optimization step, the embedded grating nanostructure's materials were varied to be investigated further. The width and the thickness of grating nanostructure would be set to 30 nm, based on the optimization of single gold grating nanostructure that has been conducted before. The SiO_2 was selected as a dielectric material based on the previous optimization step. The result of the optimization of the embedded grating nanostructure's material would be presented in Table 3.

Based on the result, we can find that the gold grating nanostructure embedded in the SiO_2 dielectric layer still provides the optimum results among the variation of the embedded grating nanostructure's material.

D. OPTIMIZATION OF THE HYDRPHOBIC LAYER'S MATERIAL

After optimizing the dielectric layer and embedded grating nanostructure's material, in this section we optimized the hydrophobic layer's material. By adding this layer, the optimization of the proposed design would be completed in this research. The setup of the complete optimization would be presented in Figure 7.

The result of the optimization of the hydrophobic layer's material would be presented in Table 4.

Based on the results obtained, it could be concluded that grating nanostructures embedded in the SiO_2 dielectric layer would achieve optimum performance when Teflon AF2400 was used instead of Teflon AF1300 and Teflon AF1601. This is possibly caused by the k value of Teflon AF2400's refractive index was lower than the other grades. It means that Teflon AF2400 exhibits a transparent characteristic so that incident light could pass through it easily rather than Teflon AF1300 and Teflon AF1601.

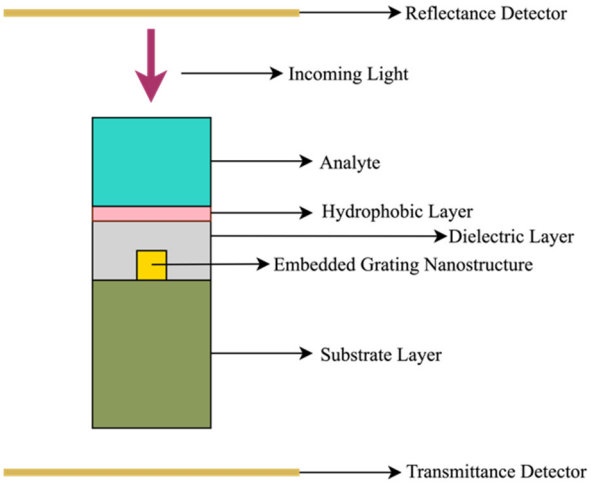

FIGURE 7. Simulation setup of the optimization of hydrophobic layer's material.

TABLE 4. Hydrophobic layer's material optimization.

Embedded Grating Nanostructure's Material	Hydrophobic's Material	Performance	
		Sensitivity (nm/RIU)	*FoM*
Au	Teflon AF1300	1406.438	1.330
	Teflon AF1601	1406.438	1.330
	Teflon AF2400	1420.937	1.352
Ag	Teflon AF1300	1241.571	1.231
	Teflon AF1601	1241.571	1.231
	Teflon AF2400	1244.799	1.238
Al	Teflon AF1300	1249.381	1.308
	Teflon AF1601	1249.381	1.308
	Teflon AF2400	1252.831	1.315
Co	Teflon AF1300	1380.646	1.45
	Teflon AF1601	1383.916	1.453
	Teflon AF2400	1387.177	1.46
Cu	Teflon AF1300	1387.414	1.449
	Teflon AF1601	1384.093	1.445
	Teflon AF2400	1390.727	1.455
Fe	Teflon AF1300	1333.048	1.474
	Teflon AF1601	1336.285	1.477
	Teflon AF2400	1336.285	1.481
Ni	Teflon AF1300	1281.258	1.392
	Teflon AF1601	1281.258	1.392
	Teflon AF2400	1287.874	1.403
Pd	Teflon AF1300	1333.631	1.393
	Teflon AF1601	1333.631	1.393
	Teflon AF2400	1340.246	1.397
Pt	Teflon AF1300	1314.003	1.393
	Teflon AF1601	1314.003	1.394
	Teflon AF2400	1320.45	1.398
Zn	Teflon AF1300	1316.739	1.395
	Teflon AF1601	1316.739	1.395
	Teflon AF2400	1323.285	1.399

However, when compared to the structure without hydrophobic material, the complete design had a slightly decreased performance represented in both sensitivity and FoM value.

It could also be concluded from the result that cobalt (Co), copper (Cu), iron (Fe), nickel (Ni), palladium (Pd), platinum (Pt), and zinc (Zn) could act as an alternative for embedded grating nanostructure's material for the proposed design other than gold (Au) because even though they had lower sensitivity rather than Au, they had higher FoM value. Also, based on some research, they had a lower price for fabrication rather than gold (Au).

TABLE 5. Comparison of performance parameter of another similar published research work.

References	Structure's Design	Performance	
		Sensitivity	*FoM*
[61]	Gold nanograting on polymethylmethacrylate (PMMA) substrate.	547 nm/RIU, 37 pmol/L (LoD)	N/A
[62]	InAsSb grating on GaSb substrate.	900 nm/RIU	0.5 to 0.6
[63]	Double bent Au strips (DAS) on polyurethane substrate.	210 nm/RIU	4.2
[64]	Gold nanograting on GaN substrate.	1140 nm/RIU	N/A
[65]	Au NPs embedded in CuO thin film.	425 nm/RIU	N/A
[66]	Au NPs embedded in TiO_2 thin film on PDMS substrate.	37.3 ± 1.5 nm/RIU	N/A
This work	Au grating nanostructure embedded in SiO_2 dielectric and coated by Teflon AF2400.	1420.937 nm/RIU	1.4
This work	Fe grating nanostructure embedded in SiO_2 dielectric and coated by Teflon AF2400.	1336.285 nm/RIU	1.5

E. THE PROFILE OF PHOTOELECTRIC CONVERSION AND MAXIMUM CURRENT DENSITY OF THE COMPLETE DESIGN

After having the complete design from the previous optimization steps, we will investigate the photoelectric conversion value and the highest current density that could be produced from the proposed design, with a variation in the embedded grating nanostructure's material. The photoelectric conversion of the proposed design with the variation of embedded grating nanostructure's material would be presented in Figure 8.

F. RESULT OBSERVATION

There was already lots of research that utilize grating nanostructure to conduct plasmonic detection for lots of kinds of

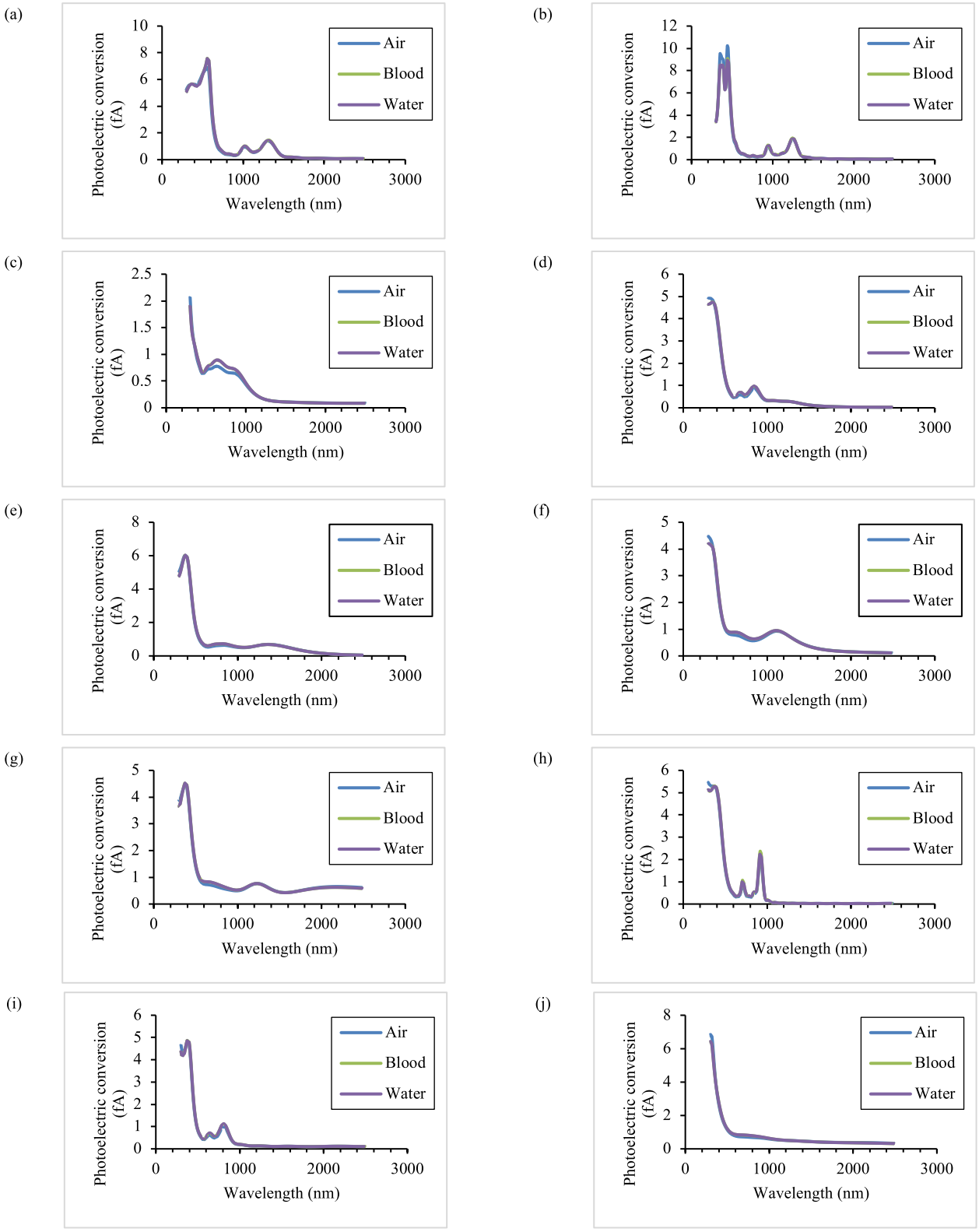

FIGURE 8. The profile of photoelectric conversion of the complete design by variating the embedded grating nanostructure's materials, such as Au (a), Ag (b), Al (c), Co (d), Cu (e), Fe (f), Ni (g), Pd (h), Pt (i), Zn (j). The dielectric and hydrophobic layer's material used were SiO_2 and Teflon AF2400, respectively.

samples. However, there were still only few research that use embedded nanostructure in dielectric design. There were some similar design structures used in some research that would be compared to this research.

IV. CONCLUSION AND FUTURE PERSPECTIVE

In this research, we've presented optimization steps when building an optical sensor system that has potential to be integrated with DMF technology. Gold nanograting structure still has the optimum performance in sensitivity, however, some other materials, such as cobalt, copper, iron, nickel, palladium, platinum, zinc, has the potential as an alternative of gold as they produce higher performance in FoM value of 1.46, 1.455, 1.481, 1.403, 1.397, 1.398, 1.399, respectively. Based on the profile of photoelectric conversion, it could be concluded that throughout the simulation wavelength, most metal materials for grating nanostructure have the maximum value under simulation wavelength of 1500 nm. The highest current density value of the proposed design by using comparison of water and blood as an analyte was obtained when the embedded grating nanostructure was made from noble metals. We believe this research could pave the next generation research of integrating optical sensor system, especially LSPR sensor, with DMF technology that could improve measurement result.

ACKNOWLEDGMENT

The authors would like to thank the Research Center for Nanosciences and Nanotechnology (RCNN), Institut Teknologi Bandung (ITB), for providing them with ANSYS Lumerical simulation tools/license to conduct this research.

REFERENCES

[1] D. E. Albert, "The growing importance of materials characterization in biocompatibility testing," *Med. Device Diagnostic Ind.*, vol. 24, no. 3, pp. 50–59, 2002.
[2] R. M. White, "A sensor classification scheme," *IEEE Trans. Ultrason., Ferroelectr., Freq. Control*, vol. UFFC-34, no. 2, pp. 124–126, Mar. 1987.
[3] Z. P. Tshabalala, D. N. Oosthuizen, H. C. Swart, and D. E. Motaung, "Tools and techniques for characterization and evaluation of nanosensors," in *Nanosensors for Smart Cities*. Amsterdam, The Netherlands: Elsevier, 2020, pp. 85–110.
[4] L. Eddaif and A. Shaban, "Fundamentals of sensor technology," in *Advanced Sensor Technology*. Amsterdam, The Netherlands: Elsevier, 2023, pp. 17–49.
[5] X. Zhu and T. Gao, "Spectrometry," in *Nano-Inspired Biosensors for Protein Assay With Clinical Applications*, Amsterdam, The Netherlands: Elsevier, 2019, pp. 237–264.
[6] J. Homola, "Surface plasmon resonance sensors for detection of chemical and biological species," *Chem. Rev.*, vol. 108, no. 2, pp. 462–493, Feb. 2008.
[7] K. M. Mayer and J. H. Hafner, "Localized surface plasmon resonance sensors," *Chem. Rev.*, vol. 111, no. 6, pp. 3828–3857, Jun. 2011.
[8] R. B. Fair, "Digital microfluidics: Is a true lab-on-a-chip possible?" *Microfluidics Nanofluidics*, vol. 3, no. 3, pp. 245–281, Jun. 2007.
[9] H. Feng, Z. Yi, R. Yang, X. Qin, S. Shen, W. Zeng, L. Shui, G. Zhou, and C. Zhang, "Designing splicing digital microfluidics chips based on polytetrafluoroethylene membrane," *Micromachines*, vol. 11, no. 12, p. 1067, Nov. 2020.
[10] B. Auguié and W. L. Barnes, "Collective resonances in gold nanoparticle arrays," *Phys. Rev. Lett.*, vol. 101, no. 14, Sep. 2008, Art. no. 143902.
[11] J. Deng, J. Du, Y. Wang, Y. Tu, and J. Di, "Synthesis of ultrathin silver shell on gold core for reducing substrate effect of LSPR sensor," *Electrochem. Commun.*, vol. 13, no. 12, pp. 1517–1520, Dec. 2011.
[12] M. Abdelgawad and A. R. Wheeler, "Low-cost, rapid-prototyping of digital microfluidics devices," *Microfluidics Nanofluidics*, vol. 4, no. 4, pp. 349–355, Apr. 2008.
[13] M. Yin, Z. Alexander Kim, and B. Xu, "Micro/nanofluidic-enabled biomedical devices: Integration of structural design and manufacturing," *Adv. NanoBiomed Res.*, vol. 2, no. 4, Apr. 2022, Art. no. 2100117.
[14] B. Hadwen, G. R. Broder, D. Morganti, A. Jacobs, C. Brown, J. R. Hector, Y. Kubota, and H. Morgan, "Programmable large area digital microfluidic array with integrated droplet sensing for bioassays," *Lab Chip*, vol. 12, no. 18, p. 3305, 2012.
[15] Z. Gu, M.-L. Wu, B.-Y. Yan, H.-F. Wang, and C. Kong, "Integrated digital microfluidic platform for colorimetric sensing of nitrite," *ACS Omega*, vol. 5, no. 19, pp. 11196–11201, May 2020.
[16] Z. Gu, J.-J. Luo, L.-W. Ding, B.-Y. Yan, J.-L. Zhou, J.-G. Wang, H.-F. Wang, and C. Kong, "Colorimetric sensing with gold nanoparticles on electrowetting-based digital microfluidics," *Micromachines*, vol. 12, no. 11, p. 1423, Nov. 2021.
[17] C. Lerma Arce, D. Witters, R. Puers, J. Lammertyn, and P. Bienstman, "Silicon photonic sensors incorporated in a digital microfluidic system," *Anal. Bioanal. Chem.*, vol. 404, no. 10, pp. 2887–2894, Dec. 2012.
[18] L. Luan, M. W. Royal, R. Evans, R. B. Fair, and N. M. Jokerst, "Chip scale optical microresonator sensors integrated with embedded thin film photodetectors on electrowetting digital microfluidics platforms," *IEEE Sensors J.*, vol. 12, no. 6, pp. 1794–1800, Jun. 2012.
[19] M. W. Royal, N. M. Jokerst, and R. B. Fair, "Droplet-based sensing: Optical microresonator sensors embedded in digital electrowetting microfluidics systems," *IEEE Sensors J.*, vol. 13, no. 12, pp. 4733–4742, Dec. 2013.
[20] H. L. Leertouwer, B. D. Wilts, and D. G. Stavenga, "Refractive index and dispersion of butterfly chitin and bird keratin measured by polarizing interference microscopy," *Opt. Exp.*, vol. 19, no. 24, pp. 24061–24066, 2011.
[21] D. G. Stavenga, H. L. Leertouwer, T. Hariyama, H. A. De Raedt, and B. D. Wilts, "Sexual dichromatism of the damselfly calopteryx japonica caused by a melanin-chitin multilayer in the male wing veins," *PLoS ONE*, vol. 7, no. 11, Nov. 2012, Art. no. e49743.
[22] G. D. Pettit and W. J. Turner, "Refractive index of InP," *J. Appl. Phys.*, vol. 36, no. 6, p. 2081, Jun. 1965.
[23] P. K. Sharma and J.-Y. Chung, "Evaluation of polydimethylsiloxane (PDMS) as a substrate for the realization of flexible/wearable antennas and sensors," *Micromachines*, vol. 14, no. 4, p. 735, Mar. 2023.
[24] V. Jain, V. Devarasetty, and R. Patrikar, "Effect of electrode geometry on droplet velocity in open EWOD based device for digital microfluidics applications," *J. Electrostatics*, vol. 87, pp. 11–18, Jun. 2017.
[25] D. Qi, K. Zhang, G. Tian, B. Jiang, and Y. Huang, "Stretchable electronics based on PDMS substrates," *Adv. Mater.*, vol. 33, no. 6, Feb. 2021, Art. no. 2003155.
[26] X. Zhang, J. Qiu, X. Li, J. Zhao, and L. Liu, "Complex refractive indices measurements of polymers in visible and near-infrared bands," *Appl. Opt.*, vol. 59, no. 8, pp. 2337–2344, 2020.
[27] M. Nania, F. Foglia, O. K. Matar, and J. T. Cabral, "Sub-100 nm wrinkling of polydimethylsiloxane by double frontal oxidation," *Nanoscale*, vol. 9, no. 5, pp. 2030–2037, 2017.
[28] A. D. Rakić, A. B. Djurišić, J. M. Elazar, and M. L. Majewski, "Optical properties of metallic films for vertical-cavity optoelectronic devices," *Appl. Opt.*, vol. 37, no. 22, pp. 5271–5283, 1998.
[29] W. S. M. Werner, K. Glantschnig, and C. Ambrosch-Draxl, "Optical constants and inelastic electron-scattering data for 17 elemental metals," *J. Phys. Chem. Reference Data*, vol. 38, no. 4, pp. 1013–1092, Dec. 2009.
[30] J. Yun, Y. H. Park, T.-S. Bae, S. Lee, and G.-H. Lee, "Fabrication of a completely transparent and highly flexible ITO nanoparticle electrode at room temperature," *ACS Appl. Mater. Interfaces*, vol. 5, no. 1, pp. 164–172, Jan. 2013.
[31] K. Choi, A. H. Ng, R. Fobel, and A. R. Wheeler, "Digital microfluidics," *Annu. Rev. Anal. Chem.*, vol. 5, pp. 413–440, Jul. 2012.
[32] H. Wang, L. Chen, and L. Sun, "Digital microfluidics: A promising technique for biochemical applications," *Frontiers Mech. Eng.*, vol. 12, no. 4, pp. 510–525, Dec. 2017.
[33] S.-K. Fan, T.-H. Hsieh, and D.-Y. Lin, "General digital microfluidic platform manipulating dielectric and conductive droplets by dielectrophoresis and electrowetting," *Lab Chip*, vol. 9, no. 9, pp. 1236–1242, 2009.
[34] R. Ghosh Chaudhuri and S. Paria, "Core/shell nanoparticles: Classes, properties, synthesis mechanisms, characterization, and applications," *Chem. Rev.*, vol. 112, no. 4, pp. 2373–2433, Apr. 2012.
[35] V. Srdic, B. Mojic, M. Nikolic, and S. Ognjanovic, "Recent progress on synthesis of ceramics core/shell nanostructures," *Process. Appl. Ceram.*, vol. 7, no. 2, pp. 45–62, 2013.
[36] O. Aguilar, S. de Castro, M. P. F. Godoy, and M. R. S. Dias, "Optoelectronic characterization of $Zn_{1-x}Cd_xO$ thin films as an alternative to photonic crystals in organic solar cells," *Opt Mater Exp.*, vol. 9, no. 9, pp. 3638–3648, 2019.

[37] D. Eya, "Deposition and characterization of PbO-PbS multilayer thin films by solution growth technique," *TURKISH J. Phys.*, vol. 38, no. 1, pp. 118–124, 2014.
[38] D. P. Kulikova, A. A. Dobronosova, V. V. Kornienko, I. A. Nechepurenko, A. S. Baburin, E. V. Sergeev, E. S. Lotkov, I. A. Rodionov, A. V. Baryshev, and A. V. Dorofeenko, "Optical properties of tungsten trioxide, palladium, and platinum thin films for functional nanostructures engineering," *Opt. Exp.*, vol. 28, no. 21, p. 32049, 2020.
[39] S. Ninomiya and S. Adachi, "Optical properties of cubic and hexagonal CdSe," *J. Appl. Phys.*, vol. 78, no. 7, pp. 4681–4689, Oct. 1995.
[40] L. V Rodríguez-de Marcos, J. I. Larruquert, J. A. Méndez, and J. A. Aznárez, "Self-consistent optical constants of SiO_2 and Ta_2O_5 films," *Opt. Mater. Exp.*, vol. 6, no. 11, pp. 3622–3637, 2016.
[41] R. E. Treharne, A. Seymour-Pierce, K. Durose, K. Hutchings, S. Roncallo, and D. Lane, "Optical design and fabrication of fully sputtered CdTe/CdS solar cells," *J. Phys., Conf. Ser.*, vol. 286, Mar. 2011, Art. no. 012038.
[42] R. Choudhary and R. P. Chauhan, "Thickness dependent variation in structural, optical and electrical properties of CdSe thin films," *J. Mater. Sci., Mater. Electron.*, vol. 30, no. 6, pp. 5753–5759, Mar. 2019.
[43] D. K. Ngwashi, T. A. Mih, and R. B. M. Cross, "The influence of ZnO layer thickness on the performance and electrical bias stress instability in ZnO thin film transistors," *Mater. Res. Exp.*, vol. 7, no. 2, Feb. 2020, Art. no. 026302.
[44] Y. Zhen, B. P. Jelle, and T. Gao, "Electrochromic properties of WO3 thin films: The role of film thickness," *Anal. Sci. Adv.*, vol. 1, no. 2, pp. 124–131, Aug. 2020.
[45] E. H. Andrews and N. A. Lockington, "The cohesive and adhesive strength of ice," *J. Mater. Sci.*, vol. 18, no. 5, pp. 1455–1465, May 1983.
[46] G. Tabatabaeipour, H. Hajghassem, and M. MohtashamiFar, "Low-cost hydrophobic layer as a top plate in two-plate digital microfluidics," *Eur. Phys. J. Appl. Phys.*, vol. 71, no. 1, p. 11101, Jul. 2015.
[47] J. B. Chae, J. O. Kwon, J. S. Yang, K. Rhee, and S. K. Chung, "Investigation on the thickness effect of a hydrophobic layer for operating voltage reduction in EWOD systems," in *Proc. IEEE 26th Int. Conf. Micro Electro Mech. Syst. (MEMS)*, Jan. 2013, pp. 1109–1112.
[48] E. Hecht, *Optics*. London, U.K.: Pearson, 2012.
[49] S. Konishi, C. Ohya, and T. Yamada, "Selective control of the contact and transport between droplet pairs by electrowetting-on-dielectric for droplet-array sandwiching technology," *Sci. Rep.*, vol. 11, no. 1, p. 12355, 2021.
[50] M. K. Yang, R. H. French, and E. W. Tokarsky, "Optical properties of Teflon AF amorphous fluoropolymers," *J. Micro/Nanolithography, MEMS MOEMS*, vol. 7, no. 3, p. 33010, 2008.
[51] D. J. Rowe, D. Smith, and J. S. Wilkinson, "Complex refractive index spectra of whole blood and aqueous solutions of anticoagulants, analgesics and buffers in the mid-infrared," *Sci. Rep.*, vol. 7, no. 1, p. 7356, 2017.
[52] G. M. Hale and M. R. Querry, "Optical constants of water in the 200-nm to 200-?m wavelength region," *Appl. Opt.*, vol. 12, no. 3, pp. 555–563, 1973.
[53] A. Mekis, S. Fan, and J. D. Joannopoulos, "Absorbing boundary conditions for FDTD simulations of photonic crystal waveguides," *IEEE Microw. Guided Wave Lett.*, vol. 9, no. 12, pp. 502–504, Dec. 1999.
[54] A. Crocherie, P. Boulenc, J. Vaillant, F. Hirigoyen, D. Hérault, and C. Tavernier , "From photons to electrons: A complete 3D simulation flow for CMOS image sensor," in *Proc. Int. Image Sensor Workshop (IISW)*, 2009, p. P15.
[55] K. Nishimura, S. Shishido, Y. Miyake, H. Kanehara, Y. Sato, J. Hirase, Y. Sato, Y. Tomekawa, M. Yamasaki, M. Murakami, M. Harada, and Y. Inoue, "Advanced features of layered-structure organic-photoconductive-film CMOS image sensor: Over 120 dB wide dynamic range function and photoelectric-conversion-controlled global shutter function," *Jpn. J. Appl. Phys.*, vol. 57, no. 10, Oct. 2018, Art. no. 1002B4.
[56] J. Zhu and G. Jin, "Performance enhancement of solar cells based on high photoelectric conversion efficiency of h-BN and metal nanoparticles," *Opt. Exp.*, vol. 30, no. 8, pp. 13469–13480, 2022.
[57] M. Sofani, M. H. Putra, and D. Djuhana, "The sensitivity calculation of localized surface plasmon resonance (LSPR) Au nanorod by applying a boundary element system simulation," *IOP Conf. Ser., Mater. Sci. Eng.*, vol. 763, no. 1, Feb. 2020, Art. no. 012076.
[58] W. Chen, H. Hu, W. Jiang, Y. Xu, S. Zhang, and H. Xu, "Ultrasensitive nanosensors based on localized surface plasmon resonances: From theory to applications," *Chin. Phys. B*, vol. 27, no. 10, Oct. 2018, Art. no. 107403.
[59] K. Lodewijks, W. Van Roy, G. Borghs, L. Lagae, and P. Van Dorpe, "Boosting the figure-of-merit of LSPR-based refractive index sensing by phase-sensitive measurements," *Nano Lett.*, vol. 12, no. 3, pp. 1655–1659, Mar. 2012.
[60] M. Bahramipanah, S. Dutta-Gupta, B. Abasahl, and O. J. F. Martin, "Cavity-coupled plasmonic device with enhanced sensitivity and figure-of-merit," *ACS Nano*, vol. 9, no. 7, pp. 7621–7633, Jul. 2015.
[61] F. Arcadio, L. Zeni, D. Montemurro, C. Eramo, S. Di Ronza, C. Perri, G. D'Agostino, G. Chiaretti, G. Porto, and N. Cennamo, "Biochemical sensing exploiting plasmonic sensors based on gold nanogratings and polymer optical fibers," *Photon. Res.*, vol. 9, no. 7, pp. 1397–1408, 2021.
[62] F. B. Barho, F. Gonzalez-Posada, M.-J. Milla-Rodrigo, M. Bomers, L. Cerutti, and T. Taliercio, "All-semiconductor plasmonic gratings for biosensing applications in the mid-infrared spectral range," *Opt. Exp.*, vol. 24, no. 14, pp. 16175–16190, 2016.
[63] J.-S. Wi, S. Lee, S. H. Lee, D. K. Oh, K.-T. Lee, I. Park, M. K. Kwak, and J. G. Ok, "Facile three-dimensional nanoarchitecturing of double-bent gold strips on roll-to-roll nanoimprinted transparent nanogratings for flexible and scalable plasmonic sensors," *Nanoscale*, vol. 9, no. 4, pp. 1398–1402, 2017.
[64] A. K. Sharma and A. K. Pandey, "Design and analysis of plasmonic sensor in communication band with gold grating on nitride substrate," *Superlattices Microstructures*, vol. 130, pp. 369–376, Jun. 2019.
[65] M. Proença, M. S. Rodrigues, F. Vaz, and J. Borges, "Carbon monoxide (CO) sensor based on Au nanoparticles embedded in a CuO matrix by HR-LSPR spectroscopy at room temperature," *IEEE Sensors Lett.*, vol. 5, no. 5, pp. 1–3, May 2021.
[66] M. S. Rodrigues, D. I. Meira, C. Lopes, J. Borges, and F. Vaz, "Preparation of plasmonic Au-TiO_2 thin films on a transparent polymer substrate," *Coatings*, vol. 10, no. 3, p. 227, Mar. 2020.

AMILLA PUSPADUHITA received the B.Sc. degree in biomedical engineering and the M.Sc. degree in nano engineering from Institut Teknologi Bandung (ITB), in 2022 and 2023, respectively. Her research interests include photonic devices and nanotechnology-related topics.

AKHMADI SURAWIJAYA (Member, IEEE) received the B.E. degree in engineering physics from Institut Teknologi Bandung (ITB), in 2001, and the M.E. degree in physical electronics from the Tokyo Institute of Technology, in 2005. He is currently a Researcher with the Device and IC Processing Laboratory, Microelectronics Center, ITB, and a Lecturer in electrical engineering with ITB. His research interests include silicon nanowires, nano devices, semiconductor fabrication processes, and photonic devices.

ISA ANSHORI received the B.Eng. degree from the Department of Engineering Physics, Institut Teknologi Bandung (ITB), Indonesia, in 2009, and the M.Eng. degree in materials science and the Ph.D. degree in nanoscience and nanotechnology from the University of Tsukuba, Japan, in 2015 and 2018, respectively. Since 2018, he has been an Assistant Professor with the Department of Biomedical Engineering, ITB. His current research interests include bio/chemical sensors, microfluidics, the IoT devices, and lab-on-chip.